Three-Dimensional Analysis of Switching Mechanism of Mixed Polymer Brushes

Denys Usov,[†] Viacheslav Gruzdev,[†] Mirko Nitschke,[†] Manfred Stamm,*[,†] Olha Hoy,[‡] Igor Luzinov,*[,‡] Ihor Tokarev,[§] and Sergiy Minko*[,§]

Leibniz-Institut für Polymerforschung Dresden e. V., Hohe Strasse 6, D-01069 Dresden, Germany, School of Materials Science and Engineering, 161 Sirrine Hall, Clemson University, Clemson, South Carolina 29634-0907, and Department of Chemistry and Bimolecular Science, Clarkson University, 8 Clarkson Avenue, Potsdam, New York 13699

Received May 14, 2007; Revised Manuscript Received August 13, 2007

ABSTRACT: The inner structure of a polystyrene−poly(methyl methacrylate) (PS/PMMA) brush synthesized via two-step surface-initiated radical polymerization was studied by a combination of step-by-step oxygen plasma etching and atomic force microscopy (AFM, "nanotomography" approach). The brush adopts ripple and dimple morphologies upon exposure to toluene and acetone, respectively. The same locations on the brush samples, adopting these two morphologies, were scanned with AFM before and after each etching step. We found that the ripple morphology consists of depressed PS-rich and elevated PMMA-rich elongated domains. In the dimple morphology, the core of the cluster is rich in PS, while the very top layer and the valleys between clusters are rich in PMMA. These experimental observations agree with self-consistent field theoretical predictions of the phase-segregated morphologies in nonselective and selective solvents. The 3D structures of the mixed brushes in dry and swollen states were reconstructed using nanotomography data.

Introduction

The goal of this work was to study a 3D arrangement of segregated polymers in a binary (mixed) polymer brush quenched by rapid evaporation of solvent. Binary polymer brushes are flexible responsive thin films capable of switching their morphologies in response to various external stimuli via different phase segregation mechanisms. Here, the term "brush" denotes a layer of polymer chains tethered to a solid substrate; the high grafting density obliges the polymers to stretch away from the grafting surface.[1] In the case of binary brushes, two different, unlike polymers are randomly grafted to the substrate.[2−6] These two polymers are segregated and form microphases which scale with the mean chain end-to-end distances.[7] Changes in the surrounding environment such as the thermodynamic quality of solvent[3,6,8,9] or humidity,[10] pH,[11] or temperature[12,13] lead to switching between various phase-segregated morphologies and affects the chemical composition of the top layer of the polymer brush. This unique behavior of polymer brushes has recently attracted great interest for various applications such as microfludic devices,[14,15] responsive colloids,[16,17] "smart" coatings,[18,19] responsive fabrics,[20] protein adsorption,[21] and supports for directed assembly of nanoparticles.[22]

Theoretical studies and simulations of binary polymer brushes have demonstrated the formation of a laterally segregated morphology in melt[23] and good solvent.[24,25] The first studies based on the self-consistent field (SCF) theory were made by Marko and Witten[26] and then by Zhulina and Balazs.[27] Employing the strong stretching approximation (when fluctuations around the chain conformation with the minimal free energy can be neglected), Marko and Witten predicted that an increase in incompatibility of the constituents (A and B) in a binary polymer brush in melt conditions causes a second-order phase transition from a disordered to a laterally segregated phase composed of A- and B-rich alternating cylindrical domains. Further increase of the incompatibility parameter should lead to the first-order transition to layered phases. Zhulina and Balazs distinguished regimes of low and high grafting density. They built a phase diagram for symmetrical conditions as a function of the grafting density and the incompatibility parameter with scaling arguments. For the brush regime, they found a homogeneous phase at low incompatibility, a periodical laterally segregated phase at higher incompatibility, and a segregated phase with diminished periodicity at very high incompatibility.

Müller extended the SCF theory for binary polymer brushes.[28,29] He expanded the binary brush composition into a set of orthonormal spatially periodic functions.[30] The free energy of the two-dimensional periodic structures was calculated within the mean field approximation and minimized with respect to their length scale. Müller predicted a second-order phase transition from the disordered to the laterally segregated state upon increase of the incompatibility of polymers in a symmetrical binary brush. The stability of a ripple phase which consists of alternating cylindrical domains of each polymer aligned parallel to the grafting surface was predicted for the symmetrical conditions in a nonselective solvent. The first-order phase transition from the ripple phase to asymmetric dimple-A and dimple-B phases was attained with changes of the conditions: selective solvent, a further increase of incompatibility of the two polymers, or a change of the brush composition to asymmetric. The dimple phases consist of round clusters of one polymer arranged in a hexagonal lattice and surrounded by the matrix of the second polymer. In selective solvents, the insoluble polymer forms clusters while the soluble polymer dominates in the surrounding matrix. On the basis of the assumption that the brush polymers are monodisperse and have equal degrees of polymerization the lateral periods of the ripple and dimple phases were estimated to be $1.85\langle r_\theta^2\rangle^{1/2}$ and $2.2\langle r_\theta^2\rangle^{1/2}$, respec-

* To whom correspondence should be addressed. E-mail: sminko@clarkson.edu (S.M.); luzinov@clemson.edu (I.L.); stamm@ipfdd.de (M.S.).
† Leibniz-Institut für Polymerforschung.
‡ Clemson University.
§ Clarkson University.

10.1021/ma071090w CCC: $37.00
Published on Web 10/24/2007

tively, where $\langle r_\theta^2 \rangle^{1/2}$ is the mean square end-to-end distance for the unperturbed polymer chains.

The experimental study of the polystyrene/poly(2-vinylpyridine) (PS/P2VP) mixed brushes with X-ray photoelectron spectroscopy (XPS) and water contact angle measurements demonstrated that the surface of the brush becomes enriched with a polymer preferred by a selective solvent to which the brush is exposed (solvophilic polymer); the brush surface becomes rich in PS after exposure to toluene and rich in P2VP after exposure to acidic water.[2,31] Thus, it was shown experimentally that a binary polymer brush exposed to a certain solvent (which is a solvent for both the polymers in the brush) and then rapidly dried (quenched) adopted (reproducibly and reversibly) the morphology which is relevant to this solvent (the morphology was not effected by all previous treatments but the last one).[8]

A good qualitative agreement between the theory and experiments was found for binary brushes poly(styrene-*co*-2,3,4,5,6-pentafluorostyrene)/poly(methyl methacrylate) (PSF/PMMA) studied with atomic force microscopy (AFM) and X-ray photoemission electron microscopy (XPEEM).[28] It was shown that the PSF/PMMA brushes adopt a ripple morphology upon exposure to the good nonselective solvent toluene and a dimple morphology upon exposure to acetone which is selective for PMMA. The authors demonstrated with XPEEM (which directly senses the local composition of the top layer of the polymer thin film) that the ripple-like morphology is formed from two kinds of alternating cylindrical domains enriched in PSF or PMMA. The XPEEM analysis of the dimple morphology showed that its top layer is dominated by PMMA and is uniform in composition. The authors concluded that (1) the structures of the experimentally observed ripple and dimple morphologies are similar to the structures of the theoretically predicted symmetric ripple and asymmetric dimple PSF (i.e., with PSF clusters) phases, respectively, and (2) the experimental ripple and dimple morphologies are stable in the solvent conditions predicted by Müller for the ripple and dimple PSF phases, respectively.

Zhao and co-workers[9] studied binary poly(methyl methacrylate)/polystyrene (PMMA/PS) brushes. They found dimple morphologies after treatment with glacial acetic acid. The XPS analysis showed an increased PMMA fraction in the top layer.

The experimental studies of the phase segregation discussed above were limited to the investigations of the top layers of the binary polymer brushes. However, they provided no sufficient evidence as to whether the experimental morphologies are relevant to the theoretically predicted 3D composition of the brush.

A report of Lemieux et al.[32] is the only exception where the mixed brushes were probed beneath the top layer using the nanoindentation method. They studied poly(styrene-*co*-2,3,4,5,6-pentafluorostyrene)/poly(methyl acrylate) (PSF/PMA) brushes using the AFM force volume mode. The contrast in mechanical properties of the polymers under ambient conditions (glassy state of PSF and rubbery state of PMA) was explored in this study. The complete change of the mechanical response in the binary brush after exposure to different selective solvents was observed in this work. The brush top layer was dominated by the glassy PSF after exposure to toluene and by the rubbery PMA after exposure to acetone. The morphologies of both the states were in good agreement with theoretical predictions; the selective solvent greatly enhanced the vertical (layering) segregation of a particular phase, while the other component collapsed into the clusters beneath.

The present work is the next step in the study of compositional profiles of mixed polymer brushes. Here, we report on the 3D binary polymer brush structure formed in different surrounding environments, quenched in a dry state by rapid evaporation of solvent, and investigated using the "nanotomography" approach[33] (step-by-step plasma etching the thin film followed by analysis of the etched surface with AFM and XPS).

Employment of nanotomography allows for a direct observation of the inner phase-segregated structures of binary polymer brushes. This method combines stepwise plasma etching with AFM studies of the polymeric films at a constant location of the scanned area before and after each etching step. Magerle[33] developed this technique using an example of a thin film of poly(styrene-*b*-butadiene-*b*-styrene), which provided a significant mechanical contrast between the glassy polystyrene and the rubbery polybutadiene domains. The domains were distinguished by phase shifts in the tapping mode. The AFM phase imaging can be used with difficulty for contrasting two glassy polymeric materials in phase-segregated films. In this case, it is still possible to distinguish between the domains of the different materials by considering changes in topography versus etching time. For example, the rate of etching of PMMA by oxygen plasma is more than two times faster than that of PS. Thus in the case of films composed of these two polymers, the PMMA-rich domains will be etched faster and transform into cavities while the PS-rich domains will be etched slower and form elevations.

Recently, we presented the results of plasma etching of PSF/PMMA brushes.[34] It was shown that the presence of fluorinated monomer units resulted in a complex phase behavior of the system. In this paper, we report on the 3D morphology for PS/PMMA mixed brush, which behaves in good agreement with theoretical predictions.

Experimental Section

Materials. Polished Si wafers (100) with natural SiO_2 layer (~2 nm) were purchased from Silchem Handelsgeselschaft mbH (Freiberg, Germany). They were washed three times with dichloromethane in an ultrasonic bath for 5 min and afterward in a mixture of water, ammonia solution (25%), and hydrogen peroxide (30%) with a volume ratio 10:1:1 at 60 °C for 1 h. The substrates were rinsed five to six times with pure water and dried with nitrogen flux. 4,4′-Azobis(4-cyanopentanoic acid) (Fluka) was used as received without additional purification. Styrene (Aldrich) and methyl methacrylate (MMA) (Aldrich) were purified on an aluminum oxide type 507C, neutral, 100−125 mesh (Fluka) chromatographic column. Toluene and tetrahydrofuran (THF) (analytical grade, Merck) were distilled by boiling over sodium for 1 h. Dichloromethane at 99.5% purity (Acros) was dried over molecular sieves overnight before use. Water was cleaned with Milli-Q ultrapure purification system, $\Omega > 18.2$ MΩ cm. Acetone (analytical grade, Merck), ammonia solution (25%, for analysis, Merck), and hydrogen peroxide (30%, stabilized, Merck) were used as received. (3-Glycidoxypropyl)trimethoxysilane (GPS, ABCR GmbH), ethylendiamine (ACROS Organics), and phosphorus pentachloride (Aldrich) were used as received. Triethylamine (Riedel-deHaën) was dried overnight over calcium hydride. Oxygen for plasma treatment with a purity of 99.95% and argon at 99.998% were purchased from Messer Griesheim, Germany.

We explored the "grafting from" method to synthesize polymer brushes using radical polymerization initiated from a solid substrate. Modification of substrates with an azo initiator and the subsequent surface-initiated polymerizations were carried out according to a general procedure reported earlier.[35] Polymerization of styrene was carried out in toluene, while MMA was polymerized in THF. The synthesis of mixed brushes was performed in two polymerization steps. Since the polymerization of the second monomer may be

affected by the brush formed by the first monomer, we prepared two series of samples with different orders of grafting: PS in the first step and PMMA in the second step (PS/PMMA), and vice versa (PMMA/PS).

Monomer solutions were purified by four freeze−pump−thaw cycles (vacuum 1.2×10^{-5} mbar). The purified solution was condensed into a glass reactor for polymerization. The Si wafer in a specially designed holder was placed into the reactor in a glovebox under Ar atmosphere (concentration of water vapors and oxygen was measured to be <1 ppm).

Characterization of the Brush Layers. Amounts of the chemisorbed azo initiator and the grafted polymers were measured with an null-ellipsometer (Multiscope, Optrel, Germany). The wavelength of the laser was 632.8 nm. The film thickness was measured at incident angle of 70°. The details of the hardware were published elsewhere.[36] For the data interpretation, we used a multilayer model of the grafted films according to the protocol described in literature.[2] For calculations, we used the following values of the refractive indices (n): 1.429 for the GPS monolayer and 1.55 as an effective value for the layer of GPS plus the attached azo initiator. For the homopolymer PS and PMMA brushes, we used values $n = 1.59$ and $n = 1.49$, respectively. Since the films of binary polymer brushes were thicker than 30 nm, the refractive indices for these polymer films were obtained directly from fitting the ellipsometric data.

The molecular weights of the grafted polymers were assumed to be the same as those for the polymers extracted from the bulk solutions.[2] The kinetic scheme for the grafting polymerization suggests that molecular weights of grafted chains and chains in the bulk are very close in values,[37,38] but in some experiments an increased molecular weight and larger polydispersity index (M_w/M_n) of the grafted polymer as compared to those of the bulk polymer were reported due to the Trommsdorff effect.[38,39] The molecular weights of the bulk PS and PMMA were determined with size exclusion chromatography using a modular built KNAUER-HPLC system (KNAUER, Germany) equipped with a refractive index detection module and two columns (PL MIXED-C, Polymer Laboratories, U.K.). PS and PMMA standards were used for calibration and THF as the effluent.

The switching behavior of the brushes in response to treatment with different organic solvents was controlled with water contact angle measurements by using equipment from Krüss GmbH, Germany. The contact angle was measured after exposure of the brushes to the solvents for 5 min followed by rapid drying with a nitrogen gun.

AFM Imaging. Imaging of the surface morphology was carried out under ambient conditions in the tapping mode at a set-point ratio 90% with a Dimension 3000 AFM microscope (Digital Instruments (DI), Inc.) equipped with an optical camera, which enabled targeting of a specified location on the sample. Phase images were obtained in the repulsive tapping mode using cantilevers with a resonant frequency of 67−87 kHz and a spring constant 1.3−3.6 N/m from Nanosensors. Cantilevers with ultrasharp tips (a radius of curvature <10 nm, a resonant frequency of 170 ± 20 kHz, and an average spring constant of 25−60 N/m) from MikroMash (Estonia) were used for topography imaging of the plasma etched samples. For analysis of the AFM data, we used the WSxM freeware downloadable from http://www.nanotec.es. The lighter color in the topographic and phase images denotes taller structures and a positive phase shift in the DI convention.[40]

The samples were scratched with a steel needle to label the selected locations on the brush surface. Since steel is harder than the polymer but softer than silicon, the polymer brush layer was removed from the scratched area while the Si substrate was not damaged. We carried out 20×20 μm^2 scans near the scratched edges to note the shape and the position of the defects in the brush layers. Afterward, we obtained 5×5 μm^2 and 2×2 μm^2 scans of the selected regions. The shape of the scratched edge and various defects in the brush layer were used to identify the same location on the sample after plasma etching. The topographic profiles of the scratches were used for determination of the thickness of the brush layer (after each etching step).

Plasma Etching. The plasma treatment was performed in a computer controlled customized MicroSys apparatus by Roth & Rau, Germany. The cylindrical vacuum chamber, made of stainless steel, had a diameter of 350 mm and a height of 350 mm. The base pressure obtained with a turbomolecular pump was $<10^{-7}$ mbar. On the top of the chamber, a 2.46 GHz ECR plasma source RR160 by Roth & Rau with a diameter of 160 mm and a maximum power of 800 W was mounted. The process gas was introduced into the active volume of the plasma source via a gas flow control system. When the plasma source was on, the pressure was measured by a capacitive vacuum gauge. The samples were introduced by a load-lock system and placed on a grounded aluminum holder near the center of the chamber. The distance between the sample and the active volume of the plasma source was about 200 mm. For the plasma treatment, the following parameters were applied: O_2 gas flow 25 sccm/min, pressure 9×10^{-3} mbar, and effective microwave power 190 W. Exposure times were specified separately for each experiment. Rates of etching for PS and PMMA spin-coated films under these conditions measured with ellipsometry were 9 and 22 nm/min, respectively.

The Si wafer with the binary brush was cut into 8×30 mm^2 pieces. Each piece was divided into several regions using labels made with a steel needle. A scratch was made with a steel needle in the middle of each region. The samples were exposed to toluene or acetone for a given period of time, allowed to dry with a nitrogen gun, and microscopic areas around the scratches were studied with AFM as described above. The sample was exposed to oxygen plasma for a certain period of time. Afterward, each marked microscopic area around the scratch was studied with AFM. The last two steps were repeated several times.

X-ray Photoelectron Spectroscopy (XPS). XPS was used to monitor the chemical composition of the outermost (8−10 nm thick) layers of polymer brush. The samples were analyzed with a Kratos AXIS 165 XPS spectrometer with an Al Kα X-ray monochromatic source (1486.6 eV). The pressure inside the analysis chamber was 5×10^{-7} Pa. The measurements were performed at a normal emission angle (90°) at pass energy of 40 eV with an energy resolution of 2 eV. Survey scans were taken in the range of 0−1200 eV. The results were analyzed with XPS commercial software.

Results

Synthesis and Characterization. We synthesized PS/PMMA and PMMA/PS layers with the grafting characteristics shown in Table 1. Distances between the grafting points (evaluated from the molecular mass of the polymer in the bulk solution and the thickness of the dry grafted layer) were much smaller than the root-mean-square (rms) end-to-end distances of PS and PMMA chains under theta conditions ($\langle r_\theta^2 \rangle^{1/2}$) and smaller than diameters of single chain globules of the polymers in the dry state ($\langle r_S^2 \rangle^{1/2}$) for all samples. Thus, the grafting density was sufficiently high for establishment of the "true" brush regime in solvents of different thermodynamic quality. The reduced tethered density (the number of chains that occupy an area that a free nonoverlapping polymer chain would normally fill at the same experimental conditions), Σ, for dry brushes is $\Sigma > 10$ ($\Sigma = \sigma\pi(\langle s^2 \rangle^{1/2})^2$, where σ is the grafting density and $\langle s^2 \rangle^{1/2}$ is the rms radius of gyration of the tethered chain at specific experimental conditions of solvent and temperature. In this work, we evaluated $\langle s^2 \rangle^{1/2}$ values according to the known procedure[41] for theta conditions using the experimental M_w values for the homopolymers.

The synthesized binary brushes adopted the ripple morphology upon exposure to toluene and the cluster-like (dimple) morphology upon exposure to acetone. The characteristic examples are shown in Figure 1. They are similar to the reported morphologies of the PSF/PMMA brushes.[7,34] The phase image

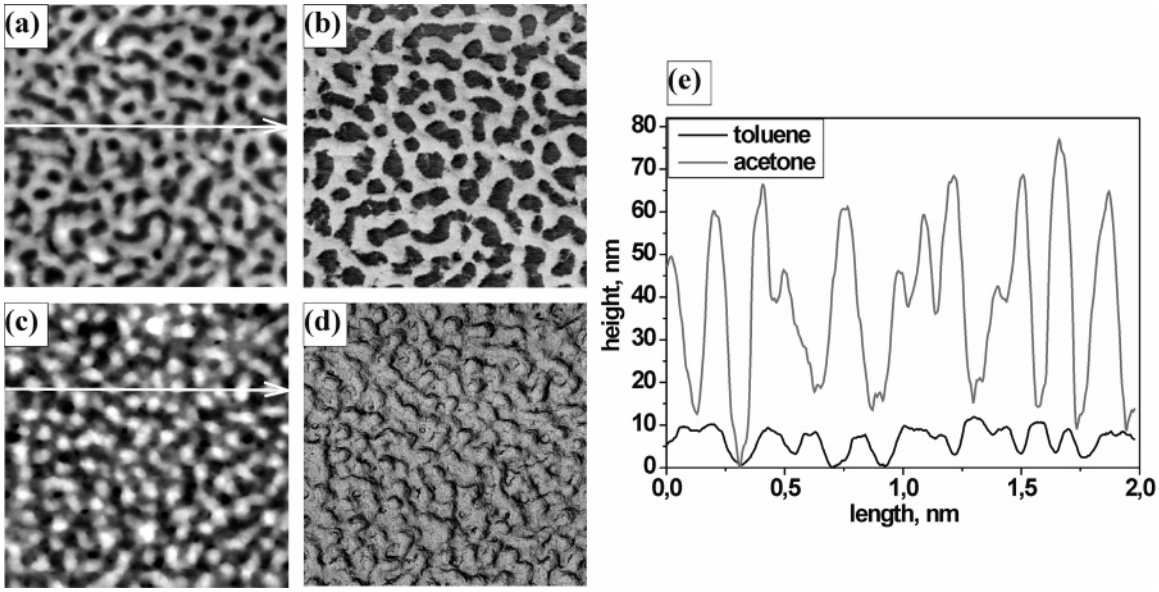

Figure 1. Representative morphologies for PMMA/PS brushes. The ripple (a,b) and dimple (c,d) morphologies (of the brush B3) adopted after 5 min exposure to toluene and acetone, respectively, and recorded in the AFM repulsive tapping mode ($2 \times 2\ \mu m^2$: topography (a,c), phase contrast (b,d)). Cross sections are shown in the panel e. White arrows in panels a and c mark the locations of the cross sections. *Z* ranges are (a) 13 nm, (b) 3.2°, (c) 78.4 nm, and (d) 27.2°.

Table 1. Characteristics of the Mixed Polymer Brushes

brush code	brush polymers (in the grafting order)	M_w (g/mol)	M_w/M_n	$\langle r_\theta^2\rangle^{1/2}$ (nm)	$\langle r_S^2\rangle^{1/2}$ (nm)	ellipsometric thickness (nm)	grafted amount (mg/m^2)	grafting density (1/nm^2)	distance between grafting points (nm)
B1	PS	364 000	1.8	40	10.4	29.9	31.4	0.052	4.9
	PMMA	787 000	1.6	57	12.8	28.7	34.4	0.026	7.0
	PS + PMMA					58.6	65.8	0.078	4.0
B2	PS	422 500	1.7	44	10.8	13.9	14.6	0.021	7.8
	PMMA	1 013 500	1.8	64	13.8	21.3	25.6	0.015	9.2
	PS + PMMA					35.2	40.2	0.036	5.9
B3	PMMA	1 013 500	1.8	64	13.8	24.8	29.8	0.018	8.5
	PS	351 600	1.6	40	10.2	12.0	12.6	0.022	7.7
	PMMA + PS					36.8	42.4	0.039	5.7

Table 2. Root-Mean-Square Roughness and Dimensions of the Lateral Structures of the Mixed Polymer Brushes after Treatment with Different Solvents

	toluene		acetone		hexane + toluene (3:1)		PS		PMMA	
brush	rms (nm)	d_r^{FFT} (nm)[a]	rms (nm)	d_d^{FFT} (nm)[a]	rms (nm)	d_r^{FFT} (nm)	d_r^{SCF} (nm)[b]	d_d^{SCF} (nm)[b]	d_r^{SCF} (nm)	d_d^{SCF} (nm)
B1	3.3	154	19.5	154			72	88	103	125
B2	2.6	111	9.8	133	31.7	182	79	97	115	141
B3	3.3	154	17.4	167	4.9	154	72	88	115	141

[a] d_d^{FFT} and d_r^{FFT} are lateral periods of the dimple and ripple morphologies, respectively, determined via fast Fourier transformation of the AFM topographic images. [b] d_r^{SCF} and d_d^{SCF} are lateral periods of the dimple and ripple morphologies, respectively, evaluated by the SCF theory.

of the ripple morphology of the brushes reported here (Figure 1b) shows that the lighter and darker regions are associated with the elevations and the depressions, respectively, in the corresponding topographic image (Figure 1a). The dimple morphology (Figure 1e, Table 2) is significantly rougher than the ripple morphology. Although the composition of the top layer should be uniform over the film surface, some contrast on the phase image is attributed to the topographic effect (Figure 1d).

The dimple morphology is obtained in acetone which is a selective solvent for PMMA. The O/C atomic concentration ratios in the top layer of the mixed brushes exposed to acetone and in the monocomponent PMMA brush are similar (Table 3), suggesting that PMMA dominates the top layer. The ripple morphology of the PS/PMMA and PMMA/PS brushes exhibits surface features with two distinct AFM phase shifts (Figure 1b), indicating lateral phase segregation of the polymers and the presence of PS- and PMMA-rich surface regions. The XPS analysis suggests a higher PS fraction in the top layer compared to that of dimple morphology (Table 3). Note, that the O/C ratio

Table 3. Surface Composition of the Mixed Polymer Brushes Exposed to Different Solvents[a]

	atom concentration (%)			
sample	O	C	Si	O/C ratio
B2 exposed to toluene	23.0	73.8	3.2	0.31
B2 exposed to acetone	25.6	73.1	1.3	0.35
B2 exposed to hexane + toluene (1:3)	8.6	90.1	1.4	0.09
B3 exposed to toluene	16.2	82.9	1.0	0.19
B3 exposed to acetone	25.4	74.6		0.34
PMMA film coated from toluene	25.3	74.1	0.6	0.34
PS coated from toluene	1.6	97.9	0.5	0.016

[a] XPS results obtained at the takeoff angle 0°.

Table 4. Water Advancing Contact Angles (Θ_{Adv}) on the Monocomponent and the Mixed Polymer Brushes after Their Treatment with Different Solvents

	Θ_{Adv} (deg) after exposure to		
brush	acetone	toluene	hexane + toluene (3:1)
PS		92 ± 1	
PMMA	75 ± 2	71 ± 2	
B2	81 ± 2	69 ± 1	120 ± 3
B3	80 ± 2	79 ± 3	92 ± 2

appears to be somewhat overestimated for the sample B2 in toluene because of contamination with SiO_2, as can be seen for the fraction of Si atoms.

It should be noted that the application of water contact angle measurements for analysis of surface composition is limited and not conclusive in this case due to the high surface roughness (rms roughness $\approx$ 20 nm) of dimple structures (Table 4). Water contact angles measured after treatment of the brushes with acetone (PMMA on the top of the brush) are higher than those measured after treatment with toluene (PS on the top). The results are in conflict with the XPS data. The contact angles after treatment with acetone are even higher than the contact angle for a homopolymer PMMA brush. Similar behavior of rough polymer brushes was reported earlier,[35] and high contact angles were observed even on hydrophilic surfaces due to surface roughness.[42]

In order to form a dimple morphology of the mixed brush in a PS-dominated surface state, we had to select a proper solvent selective for PS. Although cyclohexane is a selective solvent for PS, it is a poor solvent for PMMA. The latter may cause a kinetic barrier to approach the equilibrium morphology. Thus, we explored a mixture of *n*-hexane and toluene (3:1 vol/vol) as a solvent selective for PS and at the same time as a solvent that allows for segmental mobility of PMMA chains. Contact angle measurements provide a good contrast between the two dimple morphologies obtained from acetone and the hexane−toluene mixture (Table 4). After treatment of the brushes with a mixture of *n*-hexane and toluene (3:1 vol/vol), the XPS analysis showed a strong enrichment of the top layer of the brush B2 in PS (Table 3) while the water-advancing contact angle (Θ_{Adv}) reached 120° and 92° for the brushes B2 and B3 (Table 4), respectively. The Θ_{Adv} value obtained on the brush B2 exceeded the contact angle value for a smooth PS surface (91°) that is explained by a high surface roughness (Figure 2e).

AFM studies of the brushes B2 and B3 after treatment with a mixture of *n*-hexane and toluene (3:1 vol/vol) revealed morphologies (Figure 2) very different from the theoretically predicted dimple structure in a selective solvent. We concluded that the behavior of the film in the mixture of solvents (four-component system) differs very much from that observed for monocomponent solvents (three-component system) mainly due to the preferential absorption of good solvent in one of the brush microdomains.

We carried out the fast Fourier transformation (FFT) of the AFM topographic images to acquire average periods of laterally segregated structures in the ripple (d_r^{FFT}) and dimple (d_d^{FFT}) morphologies. The obtained values were compared with the theoretical lateral periods $d_r^{SCF} = 1.85\langle r_\theta^2\rangle^{1/2}$ and $d_d^{SCF} = 2.2\langle r_\theta^2\rangle^{1/2}$ (Table 2). The experimental lateral periods notably exceed the theoretical values evaluated using $\langle r_\theta^2\rangle^{1/2}$ for PS ($d_r^{FFT} = (1.4-2.1)d_r^{SCF}$(PS), $d_d^{FFT} = (1.4-1.9)d_d^{SCF}$(PS)) and are close to the theoretical values evaluated using $\langle r_\theta^2\rangle^{1/2}$ for PMMA ($d_r^{FFT} = (1.0-1.5)d_r^{SCF}$(PMMA), $d_d^{FFT} = (0.9-1.2)d_d^{SCF}$(PMMA)). From this analysis, we may conclude that the brush constituent with the higher degree of polymerization determines the average period of lateral segregation.

We did not observe any effect of the order of grafting on the morphology of the brushes in toluene and acetone (no difference between samples B1−B3). However, a difference between B2 and B3 samples was found upon treatment with the *n*-hexane and toluene mixture. The grafting order might affect fluctuations in the locations of grafting points and, consequently, results in a different sensitivity of the brush morphology to solvents as discussed below. Since the four-component system demonstrated a complex behavior, we excluded it from further investigation in this work.

Plasma Etching Experiments. *Ripple Structure.* For the etching experiments, we took the brush B1 with the smallest difference in the molecular weights of the polymers in the brush (Table 1). We carried out oxygen plasma etching of the brush sample which was switched to the ripple structure by exposure

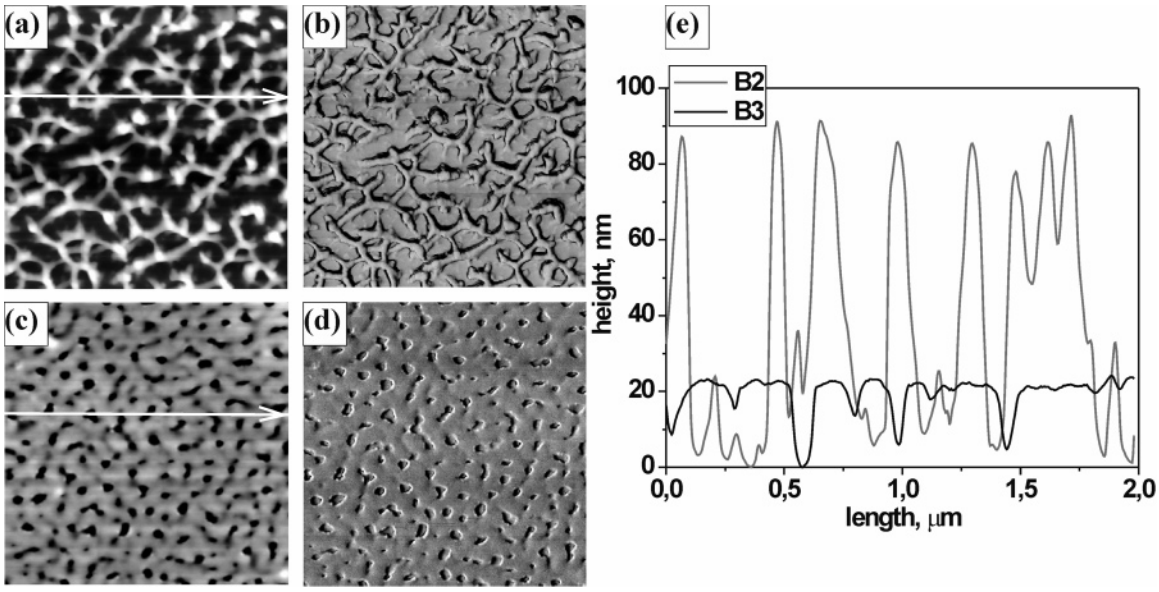

Figure 2. AFM surface morphologies ($2 \times 2\ \mu m^2$) of the brushes B2 (topography (a) phase contrast (b)) and B3 (topography (c) phase contrast (d)) after their treatment in a mixture of *n*-hexane and toluene (3:1 vol/vol). Cross sections are shown in the panel e. White arrows in panels a and c mark the locations of the cross sections. *Z* ranges are (a) 141 nm, (b) 36°, (c) 40 nm, and (d) 12°.

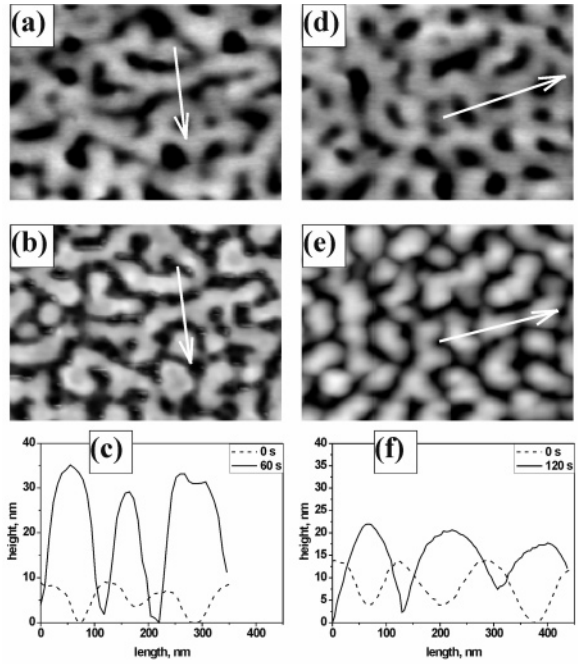

Figure 3. AFM images (tapping mode) of the brush B1 etched by oxygen plasma after 2 h exposure to toluene. The topography images ($1.00 \times 0.73\ \mu m^2$) were recorded from two locations: location 1 before etching (a) and after etching for 60 s (b), and location 2 before etching (d) and after etching for 120 s (e). The corresponding cross sections (e) and (f) illustrate the topography inversion. White arrows in panels a and c mark the locations of the cross sections.

of the brush B1 to toluene for 2 h. At zero etching time, the original morphology is a ripple morphology observed as alternating elongated (cylindrical) domains of PS and PMMA. The XPS data showed the presence of both polymers on the top layer. One polymer, however, formed bigger domains (elevations). Since the molecular weight of PMMA is higher (Table 1), we suggest that the bigger domains are formed from PMMA.

We observed an *inversion of topography* upon etching; the initially elevated features transformed to valleys as shown with two representative images obtained from two different spots on the brush sample (Figure 3). The dashed line shows the original profile of the brush (zero etching time). The solid line demonstrates the profile after 60 s etching time. Both lines match the same *x* coordinate because they were obtained from exactly the same area on the sample, as described in the experimental part. Note that the zero-height coordinate does not indicate a location of the grafting surface but shows a maximum separation between peaks of the elevations and bottoms of the valleys accessible by the AFM tip. Based on the rates of etching (PMMA was etched faster than PS), we concluded that the initially elevated features are rich in PMMA while the initial valleys are rich in PS.

The AFM topography profiles of the scratches in the brush layer are shown in Figure 4. The profile lines in this plot do not match the same position (*x* coordinate) on the sample after step-by-step etching. These plots are used to estimate an average change of the film thickness (*z* coordinate) upon etching versus the baseline indicating the location of the grafting surface (approached by the AFM tip in the scratched area). The thickness of the features of the ripple morphology was reduced from 60 to 30 nm after etching for 120 s (Figure 4a). Further etching led to elimination of PMMA and opening of the substrate (not shown).

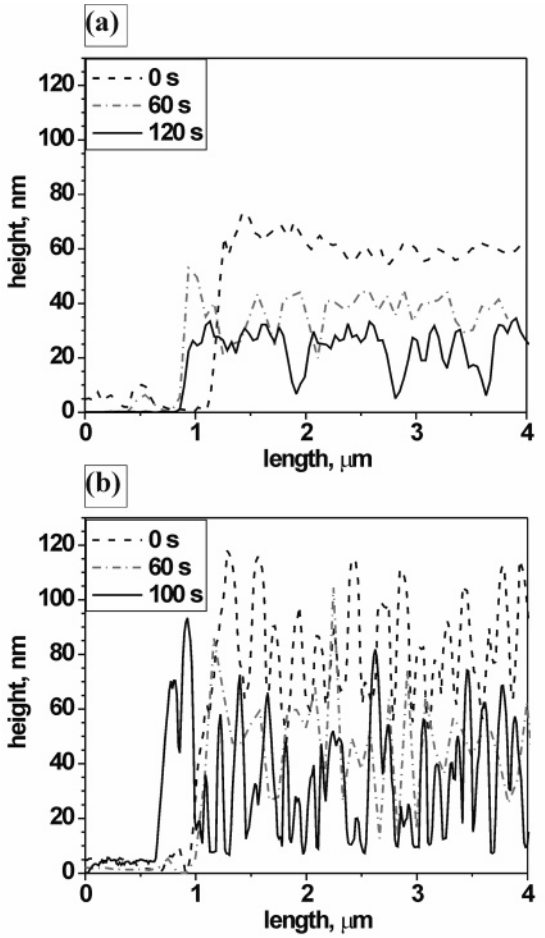

Figure 4. AFM cross sections of the ripple (a) and dimple (b) morphologies of the brush B1 upon etching (recordings near the scratched area are in the left corner of the profiles).

Scheme 1. Etching of the Ripple (a,b) and Dimple (c,d) Morphologies of the PS/PMMA Brushes[a]

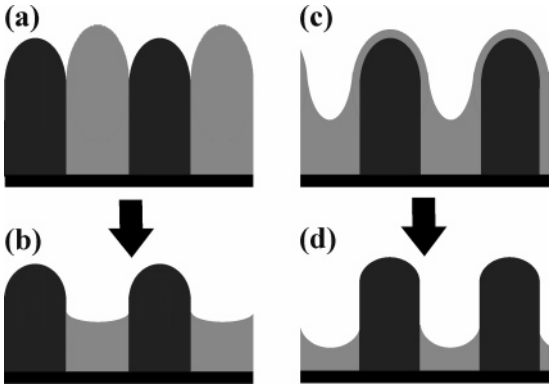

[a] PS and PMMA are schematically shown in black and gray colors, respectively. Original structures (zero etching time) are shown in the panels (a) and (c). See explanation in the text.

We reconstructed the etching process based on the rate of the film etching as shown in Scheme 1 a,b. Laterally segregated phases are shown with a dark and light contrast. PMMA domains are gray, and PS domains are black. PMMA domains form elevations, and PS domains form valleys. This topographical contrast is due to the different molecular weights of the polymers. The top image (Scheme 1a) represents the original morphology of the dry sample obtained upon exposure to a less selective solvent (toluene) and dried afterward (zero etching time). The bottom image (Scheme 1b) shows the structure for

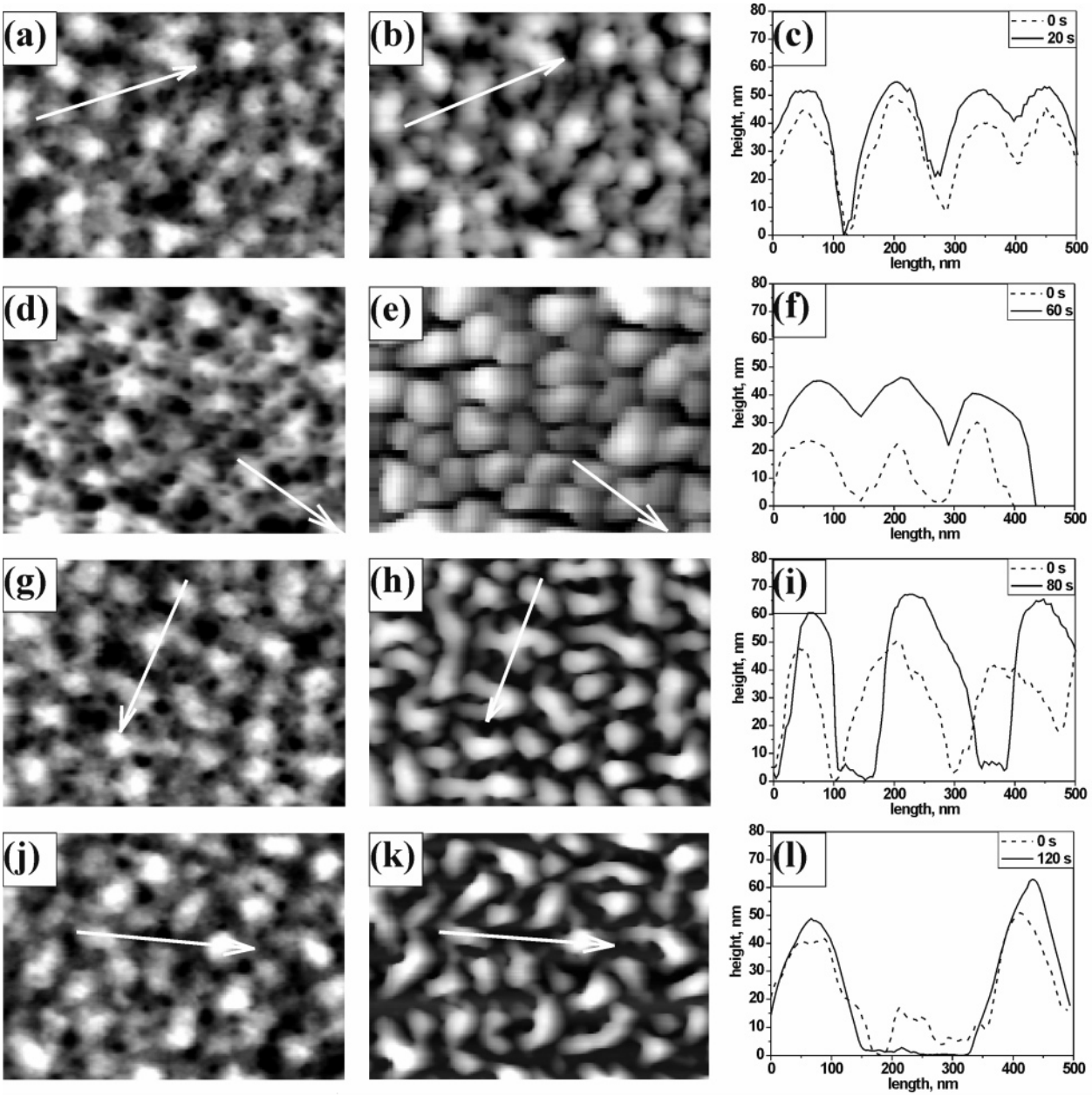

Figure 5. Oxygen plasma etching of the brush B1 after 2 h exposure to acetone. AFM topography images ($1.00 \times 0.73\ \mu m^2$) were recorded in several locations: location 1 before etching (a), after etching for 20 s (b), and the corresponding cross sections (c); location 2 before etching (d), after etching for 60 s (e), and the corresponding cross sections (f); location 3 before etching (g), after etching for 100 s (h), and the corresponding cross sections (i); location 4 before etching (j), after etching for 120 s (k), and the corresponding cross sections (l). White arrows mark the locations of the cross sections.

the same plasma etched sample. The etching rate for PMMA is higher than that for PS. Thus PMMA domains were etched faster, and we obtained an inversion of the topographical contrast. PMMA domains formed valleys and PS domains formed elevations in the etched sample.

Dimple Structure. The dimple structure obtained upon exposure of the brush B1 to acetone for 2 h (the original morphology for four different locations on the sample at zero etching time is shown in panels a, d, g, and j of Figure 5 was etched by oxygen plasma in three steps (Figure 5b,e,h,k). We observed an increase in the height of the bumps (elevations). The cross sections taken from four different locations in the sample (Figure 5c,f,i,l) show that no topography inversion was observed upon etching (in these images, the dashed lines show the original profiles at zero etching time and the solid lines show the profiles of the etched films). These data suggest a high concentration of PS in the elevated bumps and of PMMA in the valleys (since the etching of PS is slower than the etching of PMMA); this is in good agreement with the theoretical model. The change of the average layer thickness upon etching is demonstrated in Figure. 4b.

It is noteworthy that the shape of the clusters tends to change from spherical to elliptic with increasing etching time (Figured 5h,k). We assumed that a probable reason for that was the insufficient exposure to acetone, which led to incomplete formation of the phase-segregated morphology. In order to verify this, we repeated the etching experiment with another sample of the brush B1 exposed to acetone for 10 days. Again, an increase of cluster height and zero topography inversion were found upon etching (Figure 6). However, the cluster shape in the bottom of the brush layer was indeed nonspherical (Figure 6f,i). The explanation of this behavior can be obtained from a recent theoretical analysis[43] and an experimental report (so-called memory of the lateral segregation),[44] which give evidence

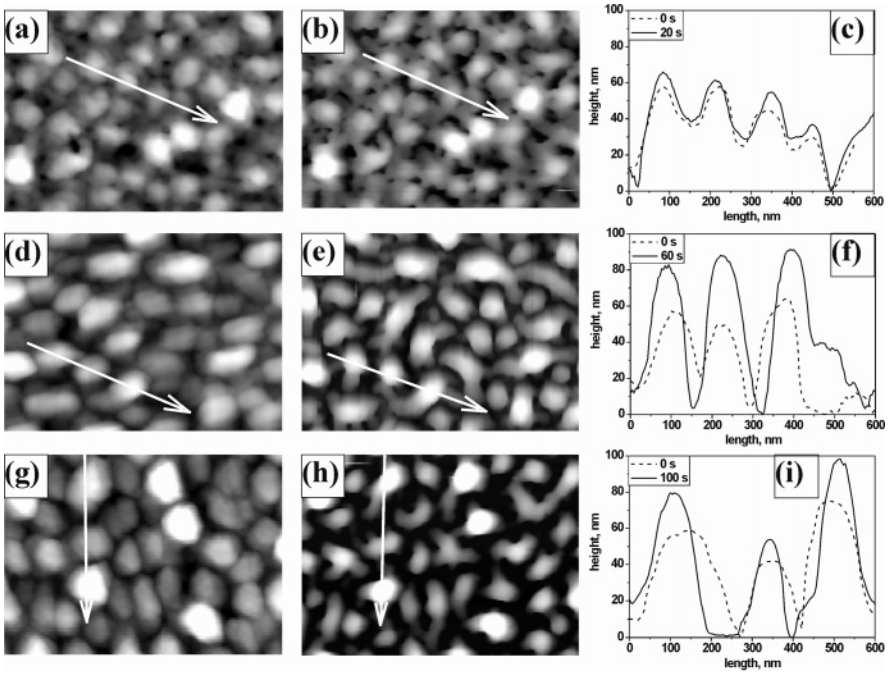

Figure 6. Oxygen plasma etching of the brush B1 after 10 days exposure to acetone. The AFM topography images (1.00 × 0.73 μm^2) were recorded at three locations: location 1 before etching (a) and after etching for 20 s (b), location 2 before etching (d) and after etching for 60 s (e), and location 3 before etching (g) and after etching for 120 s (h). The cross sections are shown in panels c, f, and i. White arrows mark the locations of the cross sections.

for a strong effect of the random character of the grafting process on the morphology of mixed brushes. It was shown that small fluctuations in the grafting points are amplified by the microphase separation and nucleate the location of the domains in the mixed brush. We suggest that small fluctuations of the grafting points affect the cluster shape more strongly near the grafting surface and that can be a reason for the shape of the elongated domains closer to the grafting surface.

As can be seen from the topographical profiles (Figures 3−6), the etching rates differ very little for the two different morphologies. Valleys formed after the topography inversion for the ripple morphology and valleys in the dimple morphology were etched with the same rate because they consist of the same polymer, PMMA. Thus, the etched films for both morphologies demonstrate similar composition profiles closer to the grafting surface, but they have different profiles at the top of the brush and have different degrees of roughness.

The reconstructed etching process and the inner structure of the dimple morphology are shown in Scheme 1c,d. The morphology of the original film (zero etching time) can be represented as a combination of the lateral and layered phase segregation of PS and PMMA (Scheme 1c). Since there is no substantial difference in the etching rates but at the same time XPS shows the enriched fraction of PMMA on top of the film, we may conclude that only a very thin layer of PMMA covers the bush. This layer is rapidly etched and afterward the morphology of the brush is represented by alternating lateral domains of the two different polymers etched with very different rates (Scheme 1d).

Discussion

The presented combination of AFM, XPS, and plasma etching was explored for the reconstruction of the 3D morphology of the etched samples of PS/PMMA mixed brushes dried (quenched) after treatment with selective and nonselective solvents. The results revealed both similarities and differences between the two morphologies formed in selective and nonselective solvents.

The similarity is in the lateral phase segregation of two polymers. Very small fluctuations in the positions of the grafting points cause a compositional inhomogeneity of the mixed brush, dictate the location of domains, and destroy long-range order in both cases. No sharp transitions between different laterally segregated morphologies were observed in the experiments. Close to the grafting surface both morphologies look very similar in structure: alternating elongated domains of PS and PMMA. This gives evidence for lateral phase segregation across the brush. For the ripple morphology, we observed no well ordered horizontally oriented cylindrical domains but rather elongated structures, which can be considered as strongly corrupted cylindrical structures.

The difference between the ripple and dimple morphologies is in the additional layered segregation in the selective solvent that results in a much higher roughness of the brush. The higher roughness of the dry sample is due to the tendency of the solvophilic polymer to cover the entire brush film. Thus, the distribution of the solvophilic PMMA between topographical domains is different in acetone and toluene as shown in Scheme 1a,c.

In the next step, on the basis of the structure of the dry films and the conclusions extracted from the SCF theory, we reconstruct the brush structure in equilibrium conditions (being swollen in solvents). In Scheme 2, we show the reconstructed swollen structures versus dry structures for both nonselective (Scheme 2a,b) and selective (Scheme 2c,d) solvents. This reconstruction was obtained by proportional swelling of both the polymers in nonselective solvent (Scheme 2a,b) and preferential swelling of the solvophilic PMMA in the selective solvent. The top of the layer in the first case appears as a ripple morphology, while a dimple morphology is expected in the second case. Below the top layer, both structures have alternating segregated phases. There is no big difference in the shape of the domains near the grafting surface. In the vicinity of the brush−solvent interface, in nonselective solvents, the domains are bent, strongly deformed cylinders (worm-like structures)

Scheme 2. Reconstruction of the Mixed Brush Morphologies in a Nonselective Solvent (a) (Shown as a Ripple Morphology with a Lateral Period d_r and the Height of the Elevations h_r),a Selective Solvent (c) (Shown as a Dimple Morphology with a Lateral Period d_d and the Height of the Elevations h_d) and in the Corresponding Dry Films (b) and (d)[a]

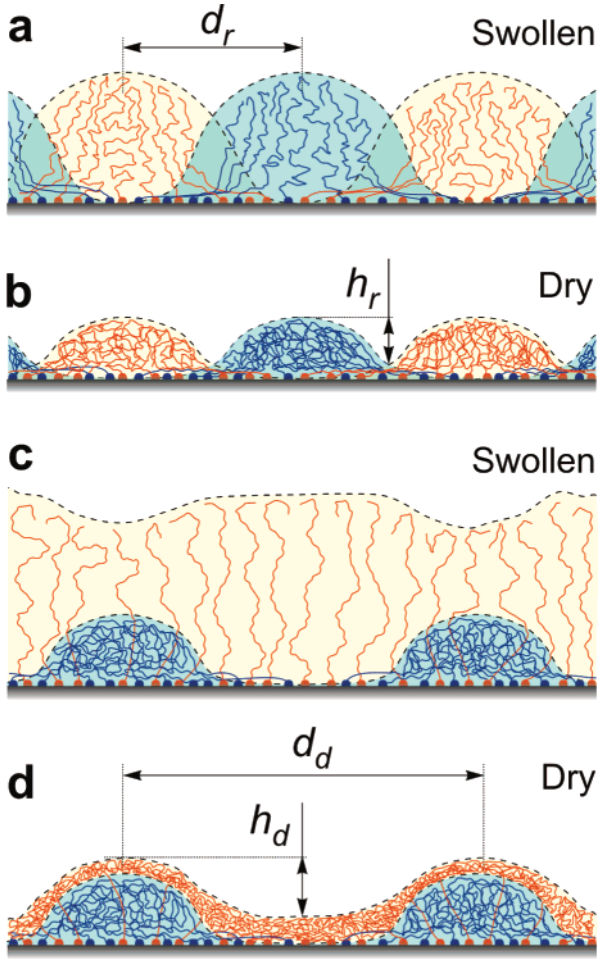

[a] $h_d > h_r$.

oriented parallel to the grafting surface while, in selective solvents, the domains of the solvophobic polymer appear as round clusters and the swollen solvophilic polymers form dimple-like structures.

Conclusions

The plasma etching experiments on the PS/PMMA brush provided information sufficient for the reconstruction of the inner structures of the mixed polymer brushes in dry and swollen states. The ripple structure formed in nonselective solvent consists of alternating PS- and PMMA-rich cylindrical domains. The dimple morphology obtained in selective solvent consists of PS-rich clusters surrounded by the PMMA-rich matrix. The top layer of the dimple morphology is dominated by PMMA. The structures of the segregated brushes upon exposure to different solvents are shown in Scheme 2c,d. Very small fluctuations in the positions of the grafting points cause a compositional inhomogeneity and destroy long-range order in both cases. In different solvents, the brushes degenerate into very similar morphologies near the grafting surface.

Acknowledgment. We acknowledge the financial support provided by DFG and NSF (Grant DMR 0602528) in the framework of the international collaborative program Materials World Network: Design of Responsive Materials via Mixed Polymer Brush Approach (D.U.). We also thank the European Graduate College "Advanced Polymeric Materials" for the financial support.

References and Notes

(1) Milner, S. T. *Science* **1991**, *251*, 905−914.
(2) Sidorenko, A.; Minko, S.; Schenk-Meuser, K.; Duschner, H.; Stamm, M. *Langmuir* **1999**, *15*, 8349−8355.
(3) Julthongpiput, D.; Lin, Y. H.; Teng, J.; Zubarev, E. R.; Tsukruk, V. V. *Langmuir* **2003**, *19*, 7832−7836.
(4) Minko, S.; Luzinov, I.; Luchnikov, V.; Muller, M.; Patil, S.; Stamm, M. *Macromolecules* **2003**, *36*, 7268−7279.
(5) Zhao, B. *Polymer* **2003**, *44*, 4079−4083.
(6) Santer, S.; Kopyshev, A.; Yang, H. K.; Ruhe, J. *Macromolecules* **2006**, *39*, 3056−3064.
(7) Minko, S.; Müller, M.; Usov, D.; Scholl, A.; Froeck, C.; Stamm, M. *Phys. Rev. Lett.* **2002**, *88*, 035502/035501−035502/035504.
(8) Minko, S.; Usov, D.; Goreshnik, E.; Stamm, M. *Macromol. Rapid Commun.* **2001**, *22*, 206−211.
(9) Zhao, B.; Haasch, R. T.; MacLaren, S. *J. Am. Chem. Soc.* **2004**, *126*, 6124−6134.
(10) Motornov, M.; Sheparovych, R.; Tokarev, I.; Roiter, Y.; Minko, S. *Langmuir* **2007**, *23*, 13−19.
(11) Houbenov, N.; Minko, S.; Stamm, M. *Macromolecules* **2003**, *36*, 5897−5901.
(12) Usov, D.; Nitschke, M.; Chitry, V.; Ulbrich, K.; Minko, S.; Stamm, M. *Abstracts of Papers*, 227th National Meeting of the American Chemical Society, Anaheim, CA, March 28−April 1, 2004; American Chemical Society: Washington, DC, 2004; PMSE 364.
(13) Motornov, M.; Sheparovych, R.; Lupitskyy, R.; MacWilliams, E.; Hoy, O.; Luzinov, I.; Minko, S. *Adv. Funct. Mater.* **2007**, in press.
(14) Ionov, L.; Houbenov, N.; Sidorenko, A.; Stamm, M.; Minko, S. *Adv. Funct. Mater.* **2006**, *16*, 1153−1160.
(15) Ionov, L.; Minko, S.; Stamm, M.; Gohy, J. F.; Jerome, R.; Scholl, A. *J. Am. Chem. Soc.* **2003**, *125*, 8302−8306.
(16) Balazs, A. C.; Singh, C.; Zhulina, E.; Chern, S. S.; Lyatskaya, Y.; Pickett, G. *Prog. Surf. Sci.* **1997**, *55*, 181−269.
(17) Motornov, M.; Sheparovych, R.; Lupitskyy, R.; MacWilliams, E.; Minko, S. *J. Colloid Interface Sci.* **2007**, *310*, 481−488.
(18) Minko, S.; Müller, M.; Motornov, M.; Nitschke, M.; Grundke, K.; Stamm, M. *J. Am. Chem. Soc.* **2003**, *125*, 3896−3900.
(19) Uhlmann, P.; Ionov, L.; Houbenov, N.; Nitschke, M.; Grundke, K.; Motornov, M.; Minko, S.; Stamm, M. *Prog. Org. Coat.* **2006**, *55*, 168−174.
(20) Motornov, M.; Minko, S.; Eichhorn, K. J.; Nitschke, M.; Simon, F.; Stamm, M. *Langmuir* **2003**, *19*, 8077−8085.
(21) Uhlmann, P.; Houbenov, N.; Brenner, N.; Grundke, K.; Burkert, S.; Stamm, M. *Langmuir* **2007**, *23*, 57−64.
(22) Santer, S.; Ruhe, J. *Polymer* **2004**, *45*, 8279−8297.
(23) Brown, G.; Chakrabarti, A.; Marko, J. F. *Europhys. Lett.* **1994**, *25*, 239−244.
(24) Lai, P. Y. *J. Chem. Phys.* **1994**, *100*, 3351−3357.
(25) Soga, K. G.; Zuckermann, M. J.; Guo, H. *Macromolecules* **1996**, *29*, 1998−2005.
(26) Marko, J. F.; Witten, T. A. *Phys. Rev. Lett.* **1991**, *66*, 1541−1544.
(27) Zhulina, E.; Balazs, A. C. *Macromolecules* **1996**, *29*, 2667−2673.
(28) Minko, S.; Muller, M.; Usov, D.; Scholl, A.; Froeck, C.; Stamm, M. *Phys. Rev. Lett.* **2002**, *88*, Art. No. 035502.
(29) Muller, M. *Phys. Rev. E* **2002**, *65*, 30802.
(30) Matsen, M. W.; Schick, M. *Phys. Rev. Lett.* **1994**, *72*, 2660−2663.
(31) Minko, S.; Patil, S.; Datsyuk, V.; Simon, F.; Eichhorn, K. J.; Motornov, M.; Usov, D.; Tokarev, I.; Stamm, M. *Langmuir* **2002**, *18*, 289−296.
(32) Lemieux, M.; Minko, S.; Usov, D.; Stamm, M.; Tsukruk, V. V. *Langmuir* **2003**, *19*, 6126−6134.
(33) Magerle, R. *Phys. Rev. Lett.* **2000**, *85*, 2749−2752.
(34) Usov, D.; Minko, S.; Nitschke, M.; Stamm, M. In *Responsive polymer materials: design and applications*; Minko, S., Ed.; Blackwell Publishing: Ames, 2006; pp 115−135.
(35) Lemieux, M.; Usov, D.; Minko, S.; Stamm, M.; Shulha, H.; Tsukruk, V. V. *Macromolecules* **2003**, *36*, 7244−7255.
(36) Motschmann, H.; Stamm, M.; Toprakcioglu, C. *Macromolecules* **1991**, *24*, 3681.
(37) Minko, S.; Gafijchuk, G.; Sidorenko, A.; Voronov, S. *Macromolecules* **1999**, *32*, 4525−4531.

(38) Luzinov, I.; Voronov, A.; Minko, S.; Kraus, R.; Wilke, W.; Zhuk, A. *J. Appl. Polym. Sci.* **1996**, *61*, 1101−1109.
(39) Boven, G.; Oosterling, M. L. C. M.; Challa, G.; Schouten, A. J. *Polymer* **1990**, *31*, 2377−2383.
(40) Magonov, S. N.; Cleveland, J.; Elings, V.; Denley, D.; Whangbo, M. H. *Surf. Sci.* **1997**, *389*, 201−211.
(41) *Polymer Handbook*, 4th ed.; John Wiley & Sons, Inc.: New York, 1999; Vol. 1, p VII/4.
(42) Extrand, C. W. *Langmuir* **2002**, *18*, 7991−7999.
(43) Wenning, L.; Muller, M.; Binder, K. *Europhys. Lett.* **2005**, *71*, 639−645.
(44) Santer, S.; Kopyshev, A.; Donges, J.; Ruhe, J.; Jiang, X. G.; Zhao, B.; Muller, M. *Langmuir* **2007**, *23*, 279−285.

MA071090W